Stability of frequency regulation of pumped-storage plants with multiple units sharing common penstock and busbar

Renbo Tang[1], Jiandong Yang[1] and Weijia Yang [1,2,*]

[1] The State Key Laboratory of Water Resources and Hydropower Engineering Science, Wuhan University, Wuhan, 430072, China
[2] Division of Electricity, Department of Engineering Sciences, Uppsala University, Uppsala, SE-751 21, Sweden

Weijia.Yang@angstrom.uu.se (Weijia Yang)

Abstract. Nowadays the frequency regulation of pumped-storage units becomes more and more important, due to the more complex structure of the grid and greater proportion of the renewable intermittent sources. The aim of this paper is to investigate the stability of pumped-storage plants (PSPs), and the subject of study is PSPs with surge tanks, shared water conduits and a common busbar. Firstly, the equations of each component in the system are deduced and simplified, to establish a linear time-invariant model by adopting the simplified transfer function (STF). A real Chinese PSP is taken as the engineering instance of this work, and simulation results of the STF model are validated with results of on-site measurements and computations based on the method of characteristics (MOC). Then, through both theoretical analysis and simulations, operating stability of the PSP system is studied under various islanded operating cases to reveal the influence of the hydraulic coupling and the electrical coupling. The results demonstrate the significant influence of the governor control modes and the parameter settings on stability of frequency regulation of the PSP. Suggestions of control strategy are also obtained.

1. Introduction

Stable and swift frequency regulation of hydropower plants (HPPs) is crucial for power systems. Especially in recent years, the amount of electricity generated by variable renewable energy sources is growing, and the regulating performance of PSPs is of great importance.

Operating stability of HPPs has been studied in the wake of vast development of hydropower industries. Stability criterion [1, 2] and eigen-analysis [3, 4] are frequently adopted for analysing stability of HPP system. While plenty of detailed models of governors, generators and loads have been proposed and implemented, studies on the complexity of hydraulic systems have also made major progress. Standard models for HPP system studies were established in [5], laying the foundation for studies involving complex hydraulic schemes. A model of two multi-machine systems with shared conduits was built and applied to study the oscillation problems during operations [6]. Three governor control modes were introduced in [7], which confirmed that control modes have very different effects on a HPP system with a surge tank. However, most of the previous works focused on single-unit HPP system, and the studies on multiple-unit system often ignored the details of hydraulic subsystem. For stability of PSPs, although considerable efforts have been made [8-10], how the hydraulic coupling affects the stability of PSPs is yet to be studied.

Hence in this paper, the object of interest is a specific type of PSP with multiple units sharing common water conduits and busbar, for analysing the influence of the hydraulic coupling and the electrical coupling. In section 2, models from former researchers are summarized and integrated to propose a STF model. In section 3, the model is validated with simulation results of MOC and on-site measurements of a real Chinese PSP. In section 4, case studies of the PSP are conducted for the stability analysis, and stability regions for various control modes with different governor settings are obtained. Finally in section 5, conclusions are condensed and suggestions for operation of PSPs are presented.

2. Model and method

Figure 1 shows a typical PSP with multiple pump-turbines installed. In this paper, a model of PSPs is established by applying STF, and equations of each component are built and presented firstly. By combining these equations, synthetic models can then be deduced. In the PSP model, two generating units share the common water conduits, indicating the hydraulic coupling; meanwhile, the two units are connected to the same busbar (sharing the same electrical load), inducing the electrical coupling. This feature of the model is a key characteristic of this paper.

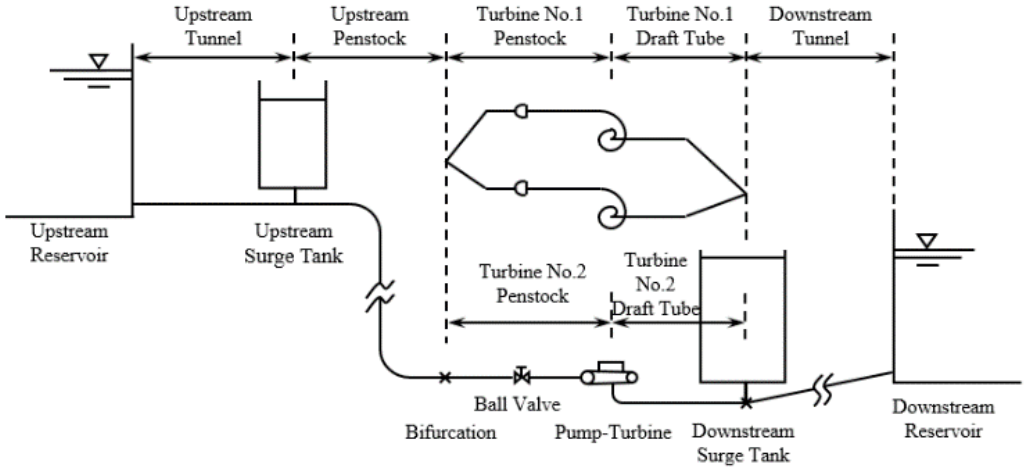

Figure 1. Layout of a pump-storage plant with shared penstock and double surge tanks

2.1. Pipeline

By neglecting minor terms and linearizing the friction term, the equation of continuity and the equation of motion can be combined and rewritten with Laplace transform [11]:

$$\frac{\Delta H_D}{\Delta Q_D}=\frac{\frac{\Delta H_U}{\Delta Q_U}-Z\tanh(\frac{l}{a}s+\frac{f\left|\bar{Q}\right|}{2DAa})}{1-\frac{\Delta H_U}{\Delta Q_U}\frac{1}{Z}\tanh(\frac{l}{a}s+\frac{f\left|\bar{Q}\right|}{2DAa})} \tag{1}$$

where $Z=a/(gA)$, $\Delta H=H-\bar{H}$, $\Delta Q=Q-\bar{Q}$.

Heads and flows at the upstream or downstream end of pipe segments are labelled with subscripts "*U*" and "*D*" respectively to indicate their location. Given a constant upstream head, i.e. ΔH_U equals zero, and normalizing change relative to rated value, equation (1) can be rewritten as:

$$G_h(s)=\frac{h}{q}=-\frac{T_w}{T_e}\tanh(T_e s+F) \tag{2}$$

where $h=\Delta H/\bar{H}$, $q=\Delta Q/\bar{Q}$, $T_w=l\bar{Q}/(g\bar{H}A)$, $T_e=l/a$.

Equation (2) is the transfer function of a one-dimensional elastic pipe, but it is still too complex to be used due to its transcendental term *tanh(s)*. Using Taylor series expansion, a polynomial

approximation is derived with a new parameter α added to fit frequency domain response to the original one [12], which here is simplified to:

$$G_f(s) = -\frac{T_w}{T_e} \cdot \frac{T_e s + F}{\alpha T_e^2 s^2 + 2\alpha F T_e s + \alpha F^2 + 1} \tag{3}$$

The best overall accuracy is achieved when α equals 0.405, and the value is used for all pipe segments thereafter. For branching junctions, two assumptions are made: 1) the summation of inflow equals the summation of outflow; 2) a common head is shared for all pipe segments at their ends connecting to the junction.

$$\begin{cases} \sum \Delta Q_U = \sum \Delta Q_{iD} \\ \Delta H_{1U} = \Delta H_{2U} = ... = \Delta H_{nU} = \Delta H_{1D} = \Delta H_{2D} = ... = \Delta H_{nD} \end{cases} \tag{4}$$

For short branch pipes adjacent to pump-turbines, (2) can be further simplified to:

$$G_r(s) = -T_w s - T_w F / T_e \tag{5}$$

Equation (5) is often referred to as the rigid column pipe transfer function. In this case, ΔQ_U equals ΔQ_D.

2.2. Pump turbine

In MOC simulations, the characteristic curve (or the characteristic surface) is the most common approach to represent the operation characteristics of a pump-turbine. In the STF model, two linearized equations are utilized instead [13]:

$$q_t = e_{qh} h_t + e_{qx} x + e_{qy} y, \tag{6}$$

$$m_t = e_h h_t + e_x x + e_y y. \tag{7}$$

where, $h_t = (\Delta H_U - \Delta H_D)/\bar{H}_t$, $q_t = \Delta Q_U/\bar{Q}_t = \Delta Q_D/\bar{Q}_t$, $x = \Delta n/\bar{n}$, $y = \Delta Y/\bar{Y}$, $m_t = \Delta M_t/\bar{M}_t$.

2.3. Governor and servomotor

A typical PID governor model and a first-order model of the servomotor are used in both MOC model and STF model [5]. In this work, automatic generation control (AGC) is considered "switched off", and thus the values of x_c, p_c and y_c are set to zero for all simulations. The transfer functions of the governor and servomotor under three control modes are shown below.

Frequency control:
$$G_{gx} = -\frac{y}{x} = -\frac{(K_D + K_P T_{1d})s^2 + (K_P + K_I T_{1d})s + K_I}{T_y T_{1d} s^3 + (T_{1d} + T_y)s^2 + s} \tag{8}$$

Power control:
$$G_{gp} = \frac{y}{p_g} \approx \frac{y}{m_t} = b_p \cdot G_{gx} \tag{9}$$

GVO control:
$$G_{gy} = 0 \tag{10}$$

2.4. Surge tank

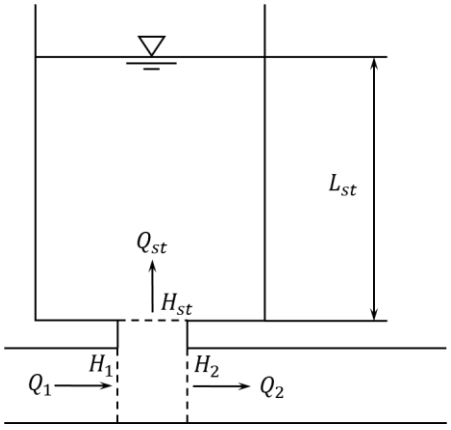

Figure 2. Diagram of a surge tank with an orifice

Surge tanks in PSPs are normally of large water inertia, which would incur simulation error if ignored. Therefore a rigid water column equation is added to form equation (11). Figure 2 shows the scheme of a surge tank and the important variables.

$$\begin{cases} Q_1 = Q_{st} + Q_2 \\ Q_{st} = c_{st}\sqrt{2g\left|H_{st} - H_1\right|} \\ \dfrac{dL_{st}}{dt} = \dfrac{Q_{st}}{A_{st}} \\ H_{st} - z - L_{st} - \dfrac{f_{st}L_{st}}{gD_{st}A_{st}^2}Q_{st}\left|Q_{st}\right| = \dfrac{2L_{st}}{gA_{st}}\dfrac{dQ_{st}}{dt} \end{cases} \tag{11}$$

Equation (11) can also be rewritten through Laplace transform as:

$$G_{st} = \frac{sA_{st}}{1 + sA_{st}(e_{st}s + F_{st})}, \tag{12}$$

where $e_{st} = \bar{L}_{st}/(gA_{st})$.

2.5. Generator and load

A concise and widely used model for generators is adopted [13], with the load self-regulation coefficient set to 0. Here, the rigid electrical connection is considered, i.e., the relative change of rotational speed of each generator equals the relative change of grid frequency. The transfer function of generator-load is:

$$\sum T_{ai} \cdot sx = \sum m_{ti} - m_g, \tag{13}$$

where $T_a = GD^2n^2/(365P)$, $m_g = \Delta M_g/\bar{M}_g$.

2.6. Overall system model

In this section, the overall system modelling is presented for STF model. The MOC model is established using the methods proposed in [11]. The block diagram of the overall system is shown in figure. 3.

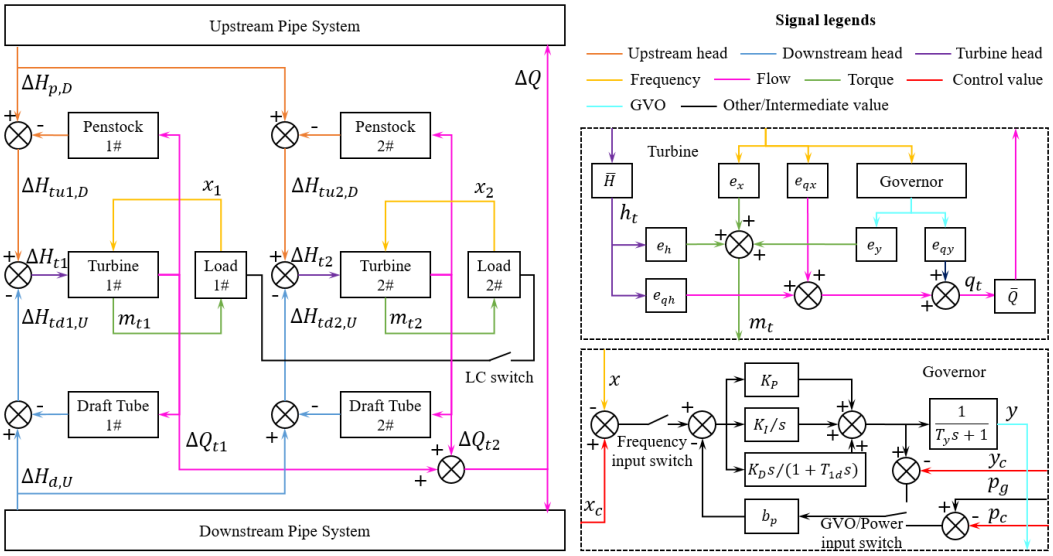

Figure 3. Transfer function diagram of the whole system

Table 1. Expressions of coefficients in system transfer functions

Control mode	Expression of A_i	Expression of B_i	Expression of I_i	Expression of J_i	Expression of C
Frequency control	$e_{qxi}+e_{qyi}\cdot G_{gxi}$	e_{qhi}	$e_{xi}+e_{yi}\cdot G_{gxi}$	e_{hi}	
Power control	$e_{qxi}+\frac{e_{qyi}e_{xi}G_{gpi}}{1+e_{yi}G_{gpi}}$	$e_{qhi}+\frac{e_{qyi}e_{hi}G_{gpi}}{1+e_{yi}G_{gpi}}$	$\frac{e_{xi}}{1+e_{yi}G_{gpi}}$	$\frac{e_{hi}}{1+e_{yi}G_{gpi}}$	$\frac{\bar{H}}{\bar{Q}}$
GVO control	e_{qxi}	e_{qhi}	e_{xi}	e_{hi}	

Combining equation (2)-(5), (6)-(10) and (12)-(13), the transfer function of turbine head can be expressed as:

$$h_{ti}=[\Delta H_{pD}-\Delta H_{dU}-q_{ti}\bar{Q}_{ti}(G_{tdi}+G_{tui})]/\bar{H}_{ti}\,, \tag{14}$$

where $\Delta H_{pD}=\sum\bar{Q}_{ti}q_{ti}\cdot G_p$, $\Delta H_{dU}=\sum\bar{Q}_{ti}q_{ti}\cdot G_d$,

$$G_p=\frac{G_u-Z_p\tanh(T_{ep}s+F_p)}{1-G_u/[Z_p\tanh(T_{ep}s+F_p)]},\ G_u=-\frac{Z_u\tanh(T_{eu}s+F_u)}{1+Z_u\tanh(T_{eu}s+F_u)\cdot G_{ust}},\ G_d=\frac{Z_d\tanh(T_{ed}s+F_d)}{1+Z_d\tanh(T_{ed}s+F_d)\cdot G_{dst}}.$$

With (6)-(8), (12)-(14), the general STF expression of the island system can be derived as:

$$\begin{cases}T_{a1}\cdot sx_1=I_1x_1+J_1h_{t1}-m_{g1}\\ T_{a2}\cdot sx_2=I_2x_2+J_2h_{t2}-m_{g2}\end{cases}. \tag{15}$$

where

$$h_{t1}=\frac{CA_1(G_w-G_{b1})[1-CB_2(G_w-G_{b2})]+C^2A_1B_2G_w^2}{[1-CB_1(G_w-G_{b1})][1-CB_2(G_w-G_{b2})]-C^2B_1B_2G_w^2}\cdot x_1+\frac{CA_2G_w[1-CB_2(G_w-G_{b2})]+C^2A_2B_2G_w(G_w-G_{b2})}{[1-CB_1(G_w-G_{b1})][1-CB_2(G_w-G_{b2})]-C^2B_1B_2G_w^2}\cdot x_2$$

$$h_{t2}=\frac{CA_1G_w[1-CB_1(G_w-G_{b1})]+C^2A_1B_1G_w(G_w-G_{b1})}{[1-CB_1(G_w-G_{b1})][1-CB_2(G_w-G_{b2})]-C^2B_1B_2G_w^2}\cdot x_1+\frac{CA_2(G_w-G_{b2})[1-CB_1(G_w-G_{b1})]+C^2A_2B_1G_w^2}{[1-CB_1(G_w-G_{b1})][1-CB_2(G_w-G_{b2})]-C^2B_1B_2G_w^2}\cdot x_2$$

The expression of each coefficient is listed in table 1.

3. Engineering case and model validation with on-site measurements

An actual PSP with the layout shown in figure 1 is applied as the engineering case of this paper. In this section, the simulation results of the STF model are validated by on-site measurements of this PSP and results through MOC simulation. The parameters of pump turbines and surge tanks are shown in table 2 and the dimensions of pipe segments are shown in table 3. Unit No.1 and No.2 share the same model

and operate at the same operation point, thus they have identical parameters, and subscripts indicating indexes are left out.

Table 2. Parameters of Simulated PSP

Turbine parameters		Surge tank parameters		Transfer coefficients		Governor parameters	
$\bar{H}_t$	540.0 m	A_{ust}	63.6 m^2	e_{qx}	-0.6557	K_P	5.0
$\bar{Q}_t$	53.4 m^3/s	e_{ust}	0.1533 s^2/ m^2	e_{qh}	0.8279	K_I	1.43
$\bar{n}$	500 r/min	A_{dst}	95.0 m^2	e_{qy}	0.9613	K_D	0.0
$\bar{P}$	309.3 MW	e_{dst}	0.3064 s^2/ m^2	e_x	-1.6896	b_P	0.04
T_a	8.7 s	\	\	e_h	1.8984	T_y	0.002s
\	\	\	\	e_y	1.1590	\	\

Table 3. Pipe Parameters of Simulated PSP

Pipe segment name	Subscript of variables	l (m)	A (m^2)	a (m/s)	Z (s/m^2)	T_e (s)	F (-)
Upstream tunnel	u	444.23	30.12	1100	3.72	0.40	0.008
Upstream penstock	p	865.69	19.95	1200	6.13	0.72	0.008
Turbine No.1 penstock	tu1	117.85	5.29	1200	23.14	0.10	0.005
Turbine No.2 penstock	tu2	108.35	5.17	1200	23.65	0.09	0.005
Turbine No.1 draft tube	td1	155.39	13.81	1200	8.12	0.14	0.005
Turbine No.2 draft tube	td2	165.89	13.89	1200	8.07	0.15	0.005
Downstream tunnel	d	1080.22	33.95	1000	3.00	1.08	0.008

The on-site measurements and simulation results of MOC and STF of unit No.1 is plotted in figure 4. Because the linearized model of pump-turbines is mainly for simulating small-disturbance cases, the STF is able to simulate the hydraulic transients of unit No.1 while not applicable for unit No.2; hence the output of unit No.2, q_{t2}, is substituted with the results from the MOC simulation. In this case, two units initially operating at rated point when unit No.2 suddenly disconnects from the grid and rejects all of its electrical load. The guide vane of unit No.2 closes in 40 s, and the ball valve shuts off in 45 s. The other unit, unit No.1 maintains operation with governor set to power control mode. Figure 4 illustrates that both MOC and STF approach can accurately emulate the water hammer effect during hydraulic transients induced by small signal disturbance, with an insignificant flaw reflecting the traveling wave effect in pipes. There are some noticeable offsets on peak times, due to the instability characteristics of pump turbines in non-optimal operation region, however the simulations still achieve a good overall accuracy. In short, the STF model is effective in reflecting the physical nature of hydraulic transients within the scope of small signal analysis.

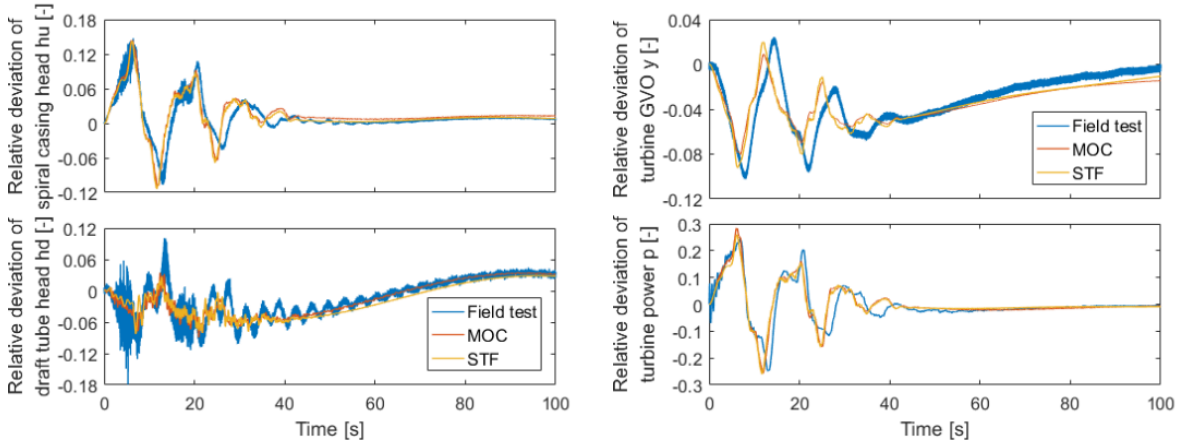

(a) Pressure in spiral case and draft tube (b) Power output and guide vane opening

Figure 4. Simulation result compared to on-site measurements of unit No.1 during a load rejection of unit No.2

4. System stability analysis

When the two units of a PSP meet the following three conditions: 1) sharing headrace and tailrace tunnels; 2) connecting to the same island grid; 3) having the symmetric layout and identical operation parameters, it can be derived that h_{t1} equals h_{t2}, and equation (15) is reduced to a single equation. The two units can be treated as one "lumped unit" with doubled Q_r, P_r and GD^2 as well as halved Z_{tu} and Z_{td}, for which plenty of relative theories are proposed and proved effective. The discussion in [14] points out explicitly how T_w and T_a affect the stability of HPPs; more specifically, a larger T_w or a smaller T_a deteriorates the stability. It is very rare that units of an actual PSP are identical, because of the different lengths in branch pipelines, the different control modes and various parameters settings. Transfer functions of such "asymmetric unit" systems are apparently different, but the general idea that T_w and T_a are the dominant coefficients still stand. For a certain PSP, its T_w and T_a are constants, and the problem now lies in what manner do governor parameters, namely K_p and K_i, exert influence on the two-unit system. To find out how exactly this affects the stability regions of these systems, multiple cases are selected and studied, as shown in table 4. It is assumed that both units are at the same operating point, and their turbine transfer coefficients are identical. For the other parameters, the default values are presented in table 2 and 3.

Table 4. Parameters and descriptions of studied cases

Index	Description	K_{p1}	K_{i1}	K_{p2}	K_{i2}	Other parameters
1	Two units adopt frequency control mode with identical governor settings, connecting to the same island grid	0.0~16.0	0.0~4.0	0.0~16.0	0.0~4.0	T_{y1}=T_{y2}=0.002s, T_{1d1}=T_{1d2}=0.02s, b_{p1} = b_{p2} = 0
2	Two units adopt frequency control mode with different K_p and K_i, connecting to the same island grid	0.0~16.0	0.0~4.0	0.0~16.0	0.0~4.0	Same as case 1
3	Unit No.1 adopts frequency control mode and No.2 adopts GVO control mode, connecting to the same island grid	0.0~16.0	0.0~4.0	\	\	Same as case 1
4	Unit No.1 adopts frequency control mode and No. 2 adopts power control mode, connecting to the same island grid	0.0~16.0	0.0~4.0	4.0	1.0	b_{p2} = 0.04, Others same as case 1

4.1. Case 1 - Both units adopt frequency control mode with identical governor settings, connecting to the same island grid

When connected to the same island grid, x_1 and x_2 can be replaced by x. The total load torque m_g is the summation of m_{g1} and m_{g2}. With equation (15), the system transfer function of x with respect to m_g can be expressed as:

$$G_{ss}(s)=\frac{x}{m_g}=\frac{1}{I_1+I_2-\dfrac{J_1h_{t1}+J_2h_{t2}}{x}-(T_{a1}+T_{a2})s} \tag{16}$$

The high-order transfer function of the system described by (16) has 15 zeros and 16 poles and cannot be solved analytically. Alternatively, all variables must be substituted with actual values in order to obtain a numerical solution. To reflect the influence of governor parameters K_p and K_i on system stability, a mesh grid of the two parameters is applied in time domain and root locus analysis. Poles and zeros of the system are shown in table 5 as a reference point (conjugate roots are recorded only once). All time domain simulations are conducted under a load step disturbance (m_g=-0.2).

In table 5, poles 1st~6th represent a series of high frequency fluctuations that relate to the traveling wave of elastic water column and other components with small time-constants. These poles are of little influence on the waveform of fluctuations due to their high frequency and damping rate. The pole 7th and 8th account for fluctuations associated with K_p and K_i. As presented in table 5, it is obvious that pole 7th has no matching zero nearby and is comparatively closer to the imaginary axis, thus it is the dominant pole of this system. The periods of fluctuations of the pole 9th and 10th match the natural period of the upstream and downstream surge tanks, and it is clear that these two poles determine the very low frequency fluctuations. In summary, poles 7th, 9th and 10th are the influential poles to this system. Figure 5 shows the frequency change in 500s with different K_p and K_i settings.

Table 5. Roots of case 1 system with referenced governor parameters*

Index	Pole (-)	Natural period (s)	Damping (-)	Nearest zero** (-)
1	-501.8371	0.0125	1.0000	-500.0000
2	-48.4940	0.1296	1.0000	-50.0000
3	-0.1572 ±13.8485	0.4537	0.0114	-0.1463 ±13.8384
4	-0.4128 ±5.3677	1.1671	0.0767	-0.3232 ±5.33720
5	-0.7141 ±3.6678	1.6815	0.1911	-0.6751 ±3.39420
6	-3.1536	1.9924	1.0000	-3.1537
7	-0.0463 ±0.6418	9.7641	0.0719	/
8	-0.2481	25.3246	1.0000	/
9	-0.0081 ±0.0966	64.7930	0.0834	-0.0105 ±0.09720
10	-0.0027 ±0.0542	115.6911	0.0503	-0.0043 ±0.05440

**The values of governor parameters K_p and K_i are 4.0 and 1.0 respectively*
***The term 'Nearest' means that the distance between this zero and its related pole is considerably smaller than any other. A '/' indicates that there is no such zero in proximity, as are the case of pole 7th and pole 8th. There are also unpaired zeros, which are -0.9213 and 0.0000.*

The influence of K_p and K_i on system response is clearly shown in figure 5. In cases with higher values of K_p and K_i, the system becomes less stable and leads to a much longer settling time. In contrast smaller values of K_p and K_i decreases the regulation rapidity, resulting in a large frequency overshoot; fluctuations in surge tanks are also aggravated, increasing the settling time. To gain a better understanding of the effect of K_p and K_i on influential poles, the root loci are plotted in figure 6 (a).

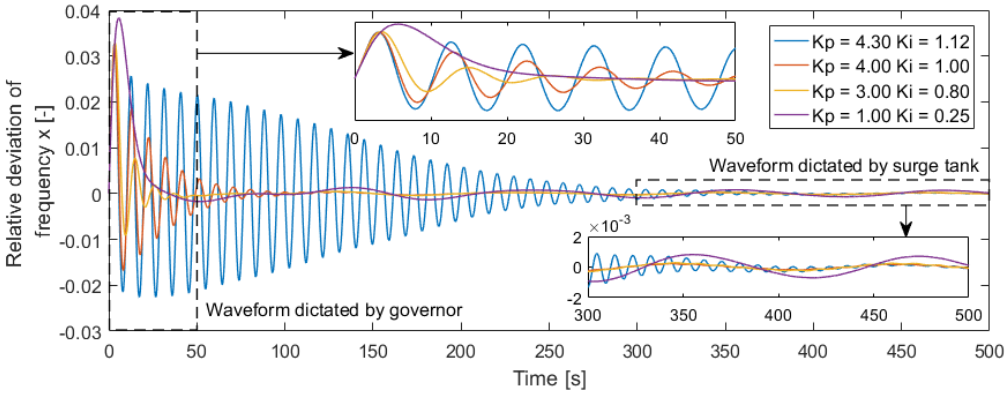

Figure 5. Frequency response to a step load with different governor parameter settings of case 1

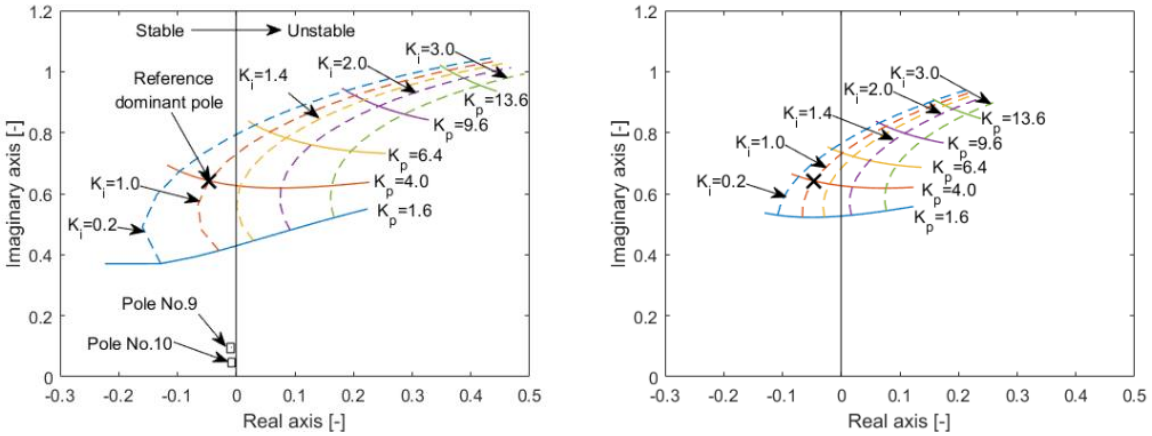

(a) Root loci of case 1 (b) Root loci of case 2

Figure 6. System root loci with respect to varying K_p and K_i in case 1 and 2

With the increase of the value of K_i, the dominant pole moves closer to the imaginary axis, reducing the damping rate of waveform dictated by the governor. The effect of K_p on the real part of the dominant pole is not monotonic as it grows when K_p increases from 1.6 to 3.0 and decreases afterwards. In figure 6, the black crosses "x" mark the dominant poles when K_p equals 4.0 and K_i equals 1.0, and the two rectangle frames delimit the trajectories of pole 9th and 10th. It is clear that pole 9th and 10th vary slightly with the change of K_p and K_i at the magnitude of 10^{-3}. This reveals that although these two parameters can be optimized to improve quality of regulation as seen in figure 5, they cannot significantly enhance the fundamental stability of oscillation in surge tanks.

4.2. Case 2, 3, 4 - Two units sharing load using different governor settings

In this section, the influence of two units in different control settings is studied. The same procedure for case 1 is executed on case 2, 3 and 4. For these three cases, equation (16) is still valid but transfer functions of governors need to be substituted according to the control mode. Trajectories of the dominant pole are plotted in figure 6 (b) and figure 7.

As illustrated in figure 6 (b) and figure 7, the black crosses "x" mark the location of the reference dominant pole. Each red cross indicates the dominant pole of the corresponding case given K_p equals 4.0 and K_i equals 1.0 for unit(s) presented in table 4. For case 2, when K_{p1} equals 4.0 and K_{i1} equals 1.0, the system is exactly the same as case 1, and the red cross coincides with the black one. Comparing (a) and (b) in figure 6, the root loci plot of case 2 appears to shrink to approximately half the size of case 1. More precisely, the distances of points on the trajectories to the reference are halved. This shrinking effect indicates that a case in which two units with different K_p and K_i is similar to one of two units with average K_p, K_i. This is also reflected in root loci of case 3, as shown in figure 7 (a). As the black 'x' lies where K_{p1} equals 7.7 and K_{i1} equals 1.8, approximately twice the value than in case 1 and case 2, while K_{p2} and K_{i2} can all be ignored as if they were 0 in GVO control mode. In other words, the effects of K_p and K_i of two units are linear. Case 4 is slightly different from case 1, 2 and 3, because the transfer function of the system has 17 zeros and 18 poles. Nevertheless, these new poles and zeros are close to each other and their effects on the system is diminished, hence the dominant pole remains unchanged. Between root loci of case 3 and 4, there is no major difference except that the latter case is more unstable with higher values of K_p and K_i. It is demonstrated that the effect of GVO control is similar with that of power control, and this is understandable that the feedback through the permanent droop has some influences on dynamic behaviour of the system. The corresponding time domain simulations are plotted in figure 8, validating the above statements.

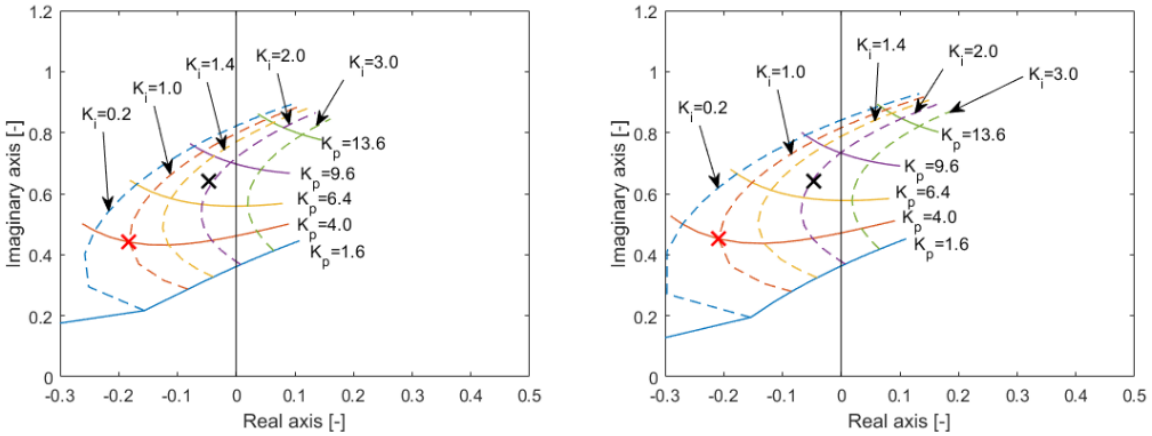

(a) Root loci of case 3 (b) Root loci of case 4

Figure 7. System root loci with respect to varying K_p and K_i of pole No.7 in case 3 and 4

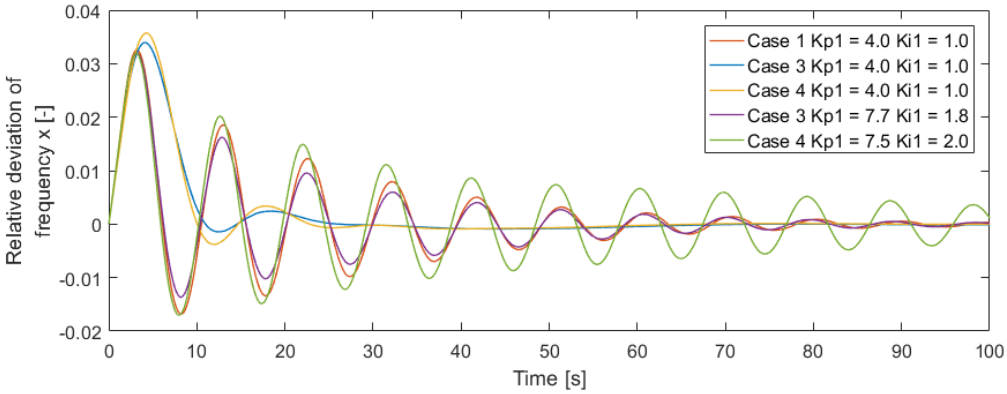

Figure 8. Frequency response to a step load with different governor settings of case 1, 3 and 4

4.3. Overall stability analysis

The stability of a linear time invariant model is determined by its dominant pole, and based on figure 6 and 7, the stability region can be presented on the same plot. As shown in figure 9, the stability boundaries of case 1, 3 and 4 are plotted wrapping the regions, and the dashed curve is created by doubling the values of K_{p1} and K_{i1} of case 1 to demonstrate the "shrinking" effect mentioned in Section 4.2.

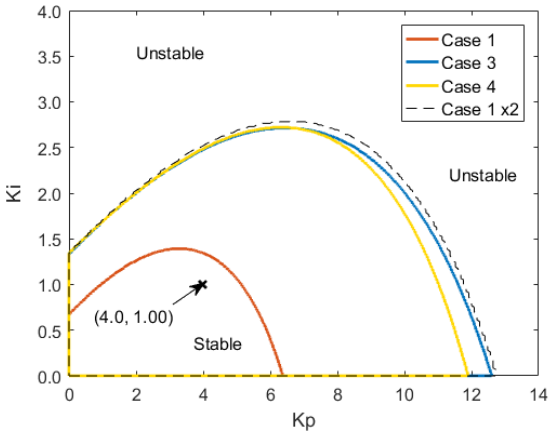

Figure 9. Stability boundaries of the PSP in different cases

5. Conclusions

In this paper, stability of PSPs with multiple units sharing common penstock and busbar is studied, and the influence of the hydraulic coupling and the electrical coupling is investigated. The conclusions of this paper are condensed as follows.

The proposed STF model is a reliable way for simulating PSPs with two coupled units, either hydraulically or electrically, and it is also suitable for theoretical analysis compared to the MOC. It can be further utilized to study small signal stability problems in PSPs with more than two units.

The stability region of the two-unit system has a similar shape to the one for one unit in parameterized plane of K_p and K_i. With larger values of K_p and K_i, the magnitude of governor control output increases, reducing maximum overshoot. However, an excessively high setting of these parameters is adverse to system stability. The stability of two units with both hydraulic coupling and electrical coupling under different values of K_p and K_i resembles that of two units with averaged values of K_p and K_i. One of the units adopting power control mode will slightly deteriorate the system stability, comparing to the case in which the unit applies GVO control mode.

Acknowledgements

The authors thank the support from the National Natural Science Foundation of China under Grant No. 51379158, and Swedish Hydropower Centre (SVC).

Nomenclatures

A	Sectional area of pipe/surge tank	h	Head change relative to nominal head
a	Pressure propagation speed in pipe	i	Imaginary unit
b_p	Governor parameters: for permanent droop	K_p	Governor parameters: for proportional term
c_{st}	Throttling factor of surge tank	K_I	Governor parameters: for integral term
D	Diameter of pipe/surge tank	K_D	Governor parameters: for differential term
D_1	Turbine diameter	L	Water level of surge tank
e_{qh}	Partial derivative of turbine flow to turbine head	$\bar{L}$	Nominal water level of surge tank
e_{qx}	Partial derivative of turbine flow to turbine speed	l	Length of pipe
e_{qy}	Partial derivative of turbine flow to turbine GVO	M	Torque

e_h	Partial derivative of turbine torque to turbine head	ΔM	Torque change
e_x	Partial derivative of turbine torque to turbine speed	m	Torque change relative to nominal torque
e_y	Partial derivative of turbine torque to turbine GVO	n	Rotational speed
e_{st}	Hydraulic inductance of surge tank	Δn	Rotational speed change
F	Lumped friction factor of pipe/surge tank	P	Power
f	Darcy-Weisbach friction factor of pipe/surge tank	p	Power change relative to nominal torque
G_h	Elastic pipe transfer function	Q	Flow
G_f	Simplified elastic pipe transfer function	ΔQ	Flow change
G_r	Rigid pipe transfer function	$\bar{Q}$	Nominal flow
G_{gx}	Governor transfer function in frequency control mode	q	Flow change relative to nominal flow
G_{gy}	Governor transfer function in GVO control mode	s	Laplace operator
G_{gp}	Governor transfer function in power control mode	T_a	Machine starting time constant
G_u	Transfer function of upstream shared tunnel	T_w	Water starting time constant
G_p	Transfer function of upstream shared penstock	T_e	Time constant of water column elasticity
G_{tu}	Transfer function of upstream branch pipe	T_{1d}	Differential filter time constant
G_{td}	Transfer function of downstream branch pipe	T_y	Time constant of guide vane servomotor
G_d	Transfer function of downstream shared tunnel	t	Time
G_{ust}	Transfer function of upstream surge tank	X	Frequency
G_{dst}	Transfer function of downstream surge tank	x	Frequency change relative to nominal value
G_{ss}	System transfer function for island grid condition	Y	Guide vane opening
GD^2	Unit inertia torque	ΔY	Guide vane opening change
g	Gravity acceleration	Z	Characteristic impedance of pipe
H	Head	z	Bottom level of surge tank
ΔH	Head change	β	Inclination angle of pipe
$\bar{H}$	Nominal head		

Subscripts

i) Indexes

i	The i-th turbine/branch pipe

ii) Abbreviations of elements

st	Variables of surge tank
t	Variables of pump-turbine

iii) Position on pipes

U	Upstream end of pipe
D	Downstream end of pipe

iv) Pipe segment abbreviations

u	Upstream tunnel
p	Upstream penstock
tu	Upstream branch pipe
td	Downstream branch pipe
d	Downstream tunnel

References

[1] Jimenez O F, Chaudhry M H and Asce M 1987 Stability Limits of Hydroelectric Power-Plants *J Energ Eng-Asce* **113** 50-60
[2] Thorne D and Hill E 1975 Extensions of stability boundaries of a hydraulic turbine generating unit *IEEE Transactions on Power Apparatus and Systems* **94** 1401-9
[3] Yu X D, Zhang J, Fan C Y and Chen S 2016 Stability analysis of governor-turbine-hydraulic system by state space method and graph theory *Energy* **114** 613-22
[4] Yang W, Norrlund P, Chi Y C, Yang J and Lundin U 2017 Eigen-analysis of hydraulic-mechanical-electrical coupling mechanism for small signal stability of hydropower plant *Renewable Energy*
[5] Demello F P, Koessler R J, Agee J, Anderson P M, Doudna J H, Fish J H, Hamm P A L, Kundur P, Lee D C, Rogers G J and Taylor C 1992 Hydraulic-Turbine and Turbine Control-Models for System Dynamic Studies *IEEE Transactions on Power Systems* **7** 167-79
[6] Pico H V, McCalley J D, Angel A, Leon R and Castrillon N J 2012 Analysis of Very Low Frequency Oscillations in Hydro-Dominant Power Systems Using Multi-Unit Modeling *IEEE Transactions on Power Systems* **27** 1906-15
[7] Guo W C, Yang J D, Chen J P, Yang W J, Teng Y and Zeng W 2015 Time Response of the Frequency of Hydroelectric Generator Unit with Surge Tank Under Isolated Operation Based on Turbine Regulating Modes *Electric Power Components and Systems* **43** 2341-55
[8] Martinez-Lucas G, Sarasua J I, Sanchez-Fernandez J A and Wilhelmi J R 2015 Power-frequency control of hydropower plants with long penstocks in isolated systems with wind generation *Renewable Energy* **83** 245-55
[9] Sarasua J I, Perez-Diaz J I, Wilhelmi J R and Sanchez-Fernandez J A 2015 Dynamic response and governor tuning of a long penstock pumped-storage hydropower plant equipped with a pump-turbine and a doubly fed induction generator *Energy Conversion and Management* **106** 151-64
[10] Martinez-Lucas G, Sarasua J I, Sanchez-Fernandez J A and Wilhelmi J R 2016 Frequency control support, of a wind-solar isolated system by a hydropower plant with long tail-race tunnel *Renewable Energy* **90** 362-76
[11] Wylie E B and Streeter V L 1978 *Fluid transients* vol 1 (New York: McGraw-Hill International Book Co.)
[12] Zeng W, Yang J D and Yang W J 2016 Instability analysis of pumped-storage stations under no-load conditions using a parameter-varying model *Renewable Energy* **90** 420-9
[13] Fang H Q, Chen L, Dlakavu N and Shen Z Y 2008 Basic Modeling and simulation tool for analysis of hydraulic transients in hydroelectric power plants *IEEE Transactions on Energy Conversion* **23** 834-41
[14] Chaudhry M H 2013 *Applied Hydraulic Transients*: Springer Science & Business Media)